Broatch, A.; Novella Rosa, R.; Garcia Tiscar, J.; Gómez-Soriano, J.; Pal, P. (2022). Investigation of the effects of turbulence modeling on the prediction of compression-ignition combustion unsteadiness. International Journal of Engine Research. 23(4):541-559. https://doi.org/10.1177/1468087421990478

Investigation of the effects of turbulence modeling on the prediction of compression-ignition combustion unsteadiness

A. Broatch[a], R. Novella[a], J. García-Tíscar[a], J. Gomez-Soriano[a,*], P. Pal[b]

[a]*CMT – Motores Térmicos, Universitat Politècnica de València, Camino de Vera, 46022 Valencia, Spain*
[b]*Energy Systems Division, Argonne National Laboratory, Lemont, IL, USA*

Abstract

Adverse effects of global warming due to the greenhouse gas emissions is changing the actual paradigm for the use energy resources. In the absence of a mid-term solution for reducing these emissions in transportation, internal combustion (IC) engines are going to coexist in the social spheres in the foreseeable future. Therefore, the study of other IC engine-related problems remains relevant to ensuring the health of the society. In this investigation, a numerical methodology for comprehensive understanding of Noise, Vibration and Harshness in internal combustion engines is proposed. Due to its inherent complexity and lack of awareness, the main objective is to evaluate the impact of the turbulence modeling framework on the in-cylinder acoustic field recreation. Modal decomposition methods have been applied to isolate the coherent flow structures and to analyze how they change with the turbulence approach. Results demonstrate that the choice of the turbulence model is a critical aspect for noise modeling. Unsteady Reynolds-Averaged Navier-Stokes schemes predict a raw estimation of the internal acoustic field with the added value of being computationally less expensive. However, the use of more complex turbulence approaches such us large eddy simulation offers an accurate prediction of the acoustic structures and their cyclic dispersion.

Keywords: *LES, NVH, acoustics, combustion unsteadiness, CFD modeling*

1. Introduction

While pollutant and greenhouse emissions are a recurring focus of regulations and research efforts, Noise, Vibration and Harshness (NVH) is traditionally addressed in the latter stages of the design process, mainly due to its inherent complexity and lack of awareness. This fact entails a large investment of resources to mitigate the undesired effects of noise in subsequent development stages or even in expensive infrastructures [1].

Within the actual paradigm, where population density and human activities increase industry demands, transportation is the main cause of noise. In particular, road traffic is by far the biggest source of noise, ahead of other external sources such as aircraft, industry or railway noise [2]. Moreover, the engine and the exhaust system are the larger sources of acoustic emissions inside the overall vehicle noise [3]. For instance, in compression-ignited (CI) powertrains, in which the combustion is particularly noisy, the powertrain can easily cover 30% of the total noise emissions [4]. Thereby, although combustion is not the sole source of noise in passenger cars, since other sources such as turbochargers, exhaust, pumps, wheels or aerodynamics are also relevant, it is certainly the most relevant one, especially in urban environments.

*Corresponding author. Tel.: +34 963 877 650,
email: jogoso1@mot.upv.es

Combustion noise results from the interaction between turbulence and combustion [5]. Traditionally, combustion noise is split into direct and indirect components [6, 7]. The direct component is linked to periodic combustion fluctuations of heat release within the flame surface [8, 9] while the indirect element is related to temperature non-uniformities which are convectively transported [9–11]. Although the overall noise emission can be constituted by both elements, the indirect noise is an exclusive feature of continuous-flux systems [12], when entropy spots are accelerated downstream of the gas turbine combustion chambers [13].

In positive displacement devices such as reciprocating internal combustion engines however, the interplay of thermal and acoustic phenomena is completely different due to their cyclic, unsteady operation, and the fact that the process occurs in a closed fluid domain. Thus, even if being merely direct noise, the ICE acoustic response is generated by different mechanisms [14–16]. On one hand, direct noise is a random phenomenon of turbulent combustion that radiates across a broadband of frequencies. On the other hand, the pressure instabilities caused by combustion are propagated as pressure waves, whose interference with the chamber walls forces the gas to oscillate in different patterns [17] and specific frequencies. This phenomenon, that may be observed as the presence of high frequency oscillations in the in-cylinder pressure or as the characteristic broad peak in the spectrum, also cited by Priede [18], is traditionally referred to as combustion chamber resonance, reverberation or even knocking.

The resonance phenomenon was firstly studied by Hickling et al. [17], who tried to improve upon purely theoretical formulas using a Finite Element Model (FEM). However, the simplicity of this model lacked the capability to resolve actual flow or combustion, or even small-scale gas oscillations. Torregrosa et al. [19] showed through calculations based on acoustic modal theory [20] how the acoustic excitation point –in this case the ignition location– has an impact on the high frequency acoustic response. Broatch et al. [21, 22] demonstrated the potential of higher complexity computational methods (CFD) for analyzing combustion chamber resonance phenomena. Wave motion across the chamber was successfully resolved and compared with theoretical cylinder modes. However, no realistic initial flow field or combustion model were used [23], introducing instead small regions of high pressure simulating the ignition points. More recent studies [24, 25] included realistic flow conditions and combustion modeling in the loop. These simulations performed under the unsteady Reynolds-Averaged Navier-Stokes (URANS) framework, despite being properly validated with lab experiments, did not strictly resolve any of the turbulent scales. Thus, the interplay between turbulence and combustion was not accurately modeled.

Although all these previous studies indicate a big push in the understanding of the in-cylinder acoustics, there is no consensus on how combustion is contributing to this phenomenon. Schuller [26] suggested that resonant oscillations are consequence of the stochastic fluctuations produced in the stabilized flame surface (non-premixed combustion). In contrast, Torregrosa, Broatch et al. [21, 25] suggest that instabilities generated during the premixed combustion are dominant in combustion chamber acoustics.

So far, a clear conclusion can not be drawn due to the uncertainties with modeling the turbulence-combustion unsteadiness responsible of NVH issues. Therefore, the use of a more complex turbulence approach such as large eddy simulation (LES) [27] could help shed some light in this regard, not only to identify all relevant phenomenology, but also to determine the optimum modeling approach.

To this end, the main objective of the present work is to identify which simulation parameters are essential for accurate prediction and analysis of combustion noise in ICE. Particularly, the impact of turbulence modeling framework on the internal acoustic field recreation is investigated in detail for the first time. Modal decomposition methods are utilized to isolate the coherent flow structures and to analyze how they change with the selected turbulence approach, thereby giving a quantitative view of the most relevant phenomena. The paper is organized as follows. The numerical methodology is presented in Section 2 including details of numerical model setup and post-processing methods used. Section 3 shows the validation of the numerical model. Section 4 discusses the main findings of this study. Finally, the main conclusions are drawn in Section 5.

Table 1: *Main specifications and injection system characterization of the engine.*

Engine type	**CI diesel engine**
Number of cylinders [-]	4 in line
Displacement [cm^3]	1600
Bore - Stroke [mm]	75.0 - 88.3
Connecting rod length [mm]	13.7
Compression ratio [-]	18:1
Number of valves [-]	2 intake and 2 exhaust
Injector nozzles	6
Nozzle holes diameter [μm]	124
Included spray angle [deg]	150

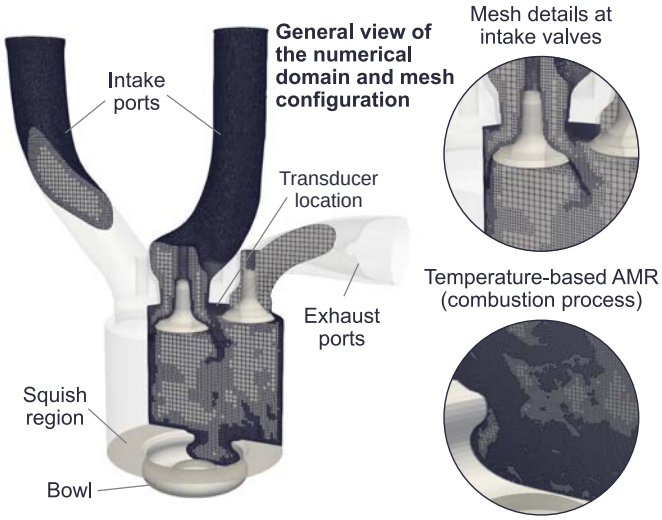

Figure 1: *Numerical domain and mesh characterization of the engine architecture.*

2. Methodology

The numerical methodology developed for this investigation is based on a CFD model of a CI engine. The main characteristics of the engine are summarized in Table 1.

2.1. CFD model setup

The unsteady flow field was assessed by the CFD code CONVERGE [28]. The numerical solution was computed through the finite volume method. The species transport was calculated by the mass fraction governing equations of all considered species. A second-order central difference scheme for both convective and diffusive terms was used for spatial discretization and a first-order implicit scheme was employed for temporal discretization.

The internal energy equation is also solved in its compressible form with the help of the Redlich-Kwong equation of state [29]. Pressure-velocity coupling was achieved by using a modified Pressure Implicit with Splitting of Operators (PISO) method [30].

Two different turbulence schemes were used in this investigation. On one hand, LES [31] was used to approach the turbulence problem by performing a low-pass spatial filtering of the Navier-Stokes equations. The LES subgrid scale tensor is modelled using the one-equation dynamic structure model

[32, 33] in which the transport equation for the subgrid kinetic energy is calculated with an additional transport equation. On the other hand, the turbulent field was also modeled using URANS-based renormalized group (RNG) $k-\varepsilon$ model [34]. This approach showed a good performance when simulating spray and combustion features in previous studies [35, 36]. Both turbulence approaches were coupled with the wall heat transfer model developed by Angelberger et al. [37] for the near-wall modelling. This model accounts for both quasi-isothermal and non-isothermal wall flows, being suitable for internal combustion engine applications.

For combustion modeling, the finite-rate chemistry solver [38] was employed along with a multi-zone (MZ) approach, with bins of 5 K in temperature and 0.05 in equivalence ratio [39]. Although it does not utilize an explicit turbulent combustion closure [40, 41], this approach model in combination with an adequate cells size has been demonstrated to perform well for simulating spray combustion in the context of both RANS and LES in previous studies [36, 42].

A chemical kinetic mechanism for primary reference fuels (PRF) based on Brakora et al. [43] was used in this work to account for fuel chemistry and n-heptane was used as the diesel surrogate.

The fuel injection was described by the standard Discrete Droplet Model (DDM) [44]. Kelvin Helmholtz (KH)-Rayleigh Taylor (RT) breakup model was employed to model spray atomization [45]. Droplet collision and coalescence were modeled by O'Rourke's model [46]. Moreover, the Frossling correlation [47] was used to model fuel evaporation. The drag coefficient of the droplets was calculated by the dynamic drag model of Liu et al. [48]. All calibration constants were set by their respective fundamental investigations [44–48].

Following the extensively accepted standard approach [49], diesel fuel physical properties were given by the *diesel2* fuel surrogate [50], which is known to provide suitable estimations of key spray parameters such as liquid length [50].

Cylinder wall temperatures were assumed to be constant and estimated using a lumped heat transfer model [51]. The inflow/outflow boundaries placed at the end of the intake and exhaust ports were prescribed by the cycle-averaged values of the corresponding measured pressures and temperatures.

As can be seen in Fig. 1, the numerical domain included the complete single cylinder geometry and the intake/exhaust ports, allowing to perform full cycle simulations. The mesh discretization was done using the cut-cell Cartesian method. The base mesh size was fixed throughout the domain depending on the turbulence scheme used. Complete details about the mesh resolution are included in Table 2 for the two model setups. Both configurations have essentially the same setup with only few changes in the grid resolution to achieve a better compliance with the requirements of the two used turbulence approaches.

The mesh size for the URANS simulations was obtained after extensive research published in various articles [24, 52, 53]. In all these papers, the numerical solution was widely validated and analyzed with a base cell and AMR sizes of 3 and 0.375 mm, respectively.

Due to the lack of an explicit turbulent combustion closure, the LES mesh resolution was increased taking into account the recommendations found in the literature [33, 54] in order to solve all relevant flow structures in the domain. The mesh was refined up to 0.275 mm in the walls of the combustion chamber, ports and the region near the fuel injector, to deal with the requirements of the boundary layer, the spray atomization and droplet breakup/coalescence approaches. Mesh size in the chamber was reduced to 0.55 mm after the start of combustion, for an improved prediction of the interaction and reflection of the pressure waves while avoiding undesired spatial aliasing effects. The code also employed adaptive mesh refinement (AMR) to increase grid resolution up to 0.138 mm based on the velocity and temperature subgrid scales.

This mesh configuration was selected after a broad literature review. In this task, recommendations about the grid resolution [38, 55–58] and temporal discretization [19, 22] were taken into account in order to adequately capture the main features of diesel combustion [59, 60] and its subsequent unsteady pressure oscillations [61, 62].

A monitor point located at the same position as the pressure transducer (Fig. 1) in the experiments was used to compare the experimental and simulated data for validation. These signals were recorded at a sampling frequency of 50 kHz so as to provide an aliasing-free bandwidth, sufficient to cover the human hearing range [63].

2.2. Post-processing methods

Apart from qualitative and quantitative comparisons of local and global variables, other specific methods were used for the analysis and validation of the numerical results.

For example, the analysis of the flow through the engine gas exchange is fundamentally based on the comparison of the resulting non-reacting flow field. In order to do this, a direct visualization of the velocity field was used, but also some additional parameters were calculated to quantify the intensity of the flow movement in a given preferential direction –in this case the characteristic swirl movement of the flow– and the position of the vortex associated with it. The swirl intensity (also named averaged swirl ratio or SR) can be estimated by dividing the mean angular velocity of the gas inside the combustion chamber at the number of measuring points, and the crankshaft angular velocity. The vortex center position is directly derived from the topology of the velocity field [64]. The method to identify this location is based on the work of Grosjean et al. [65]. Based on a combination of LDA (Laser Doppler anemometry) and PIV (Particle image velocimetry) measurements, they defined a scalar function that locates the vortex core when it approximates to zero. Full details about this method can be found in [64, 65].

On the other hand, the effects of combustion on the internal acoustic field were quantified with the help of the modal decomposition technique. Particularly, Proper Orthogonal Decomposition (POD), also known as Principal Component analysis (PCA) and Karhunen–Loève expansion [66], was utilized to isolate the most coherent flow structures and understand

Table 2: *Mesh details about the different model configurations used.*

Configuration	URANS	LES	Activation period
Base size	3 mm	2.2 mm	Permanent
Walls refinement	0.375 mm	0.275 mm	Permanent
Spray refinement	0.375 mm	0.275 mm	[-40.0 – 40.0] deg
Chamber refinement	0.75 mm	0.55 mm	[-100.0 – 100.0] deg
AMR min. size	0.188 mm	0.138 mm	Permanent
Turbulence modeling	URANS RNG k-ϵ	Dynamic structure LES	–
Number of cells	2-8 million	13-25 million	–

which ones contribute to the acoustics to a larger extent. The origin of this method can be found in the field of probability theory [67] and its objective is to decompose the flow field into a sum of paired spatial and temporal modes. POD can be performed gathering time-snapshots of a system as columns of a matrix $\mathbf{V}$ and then directly solving[68] the eigensystem associated with the time-averaged spatial correlation matrix $\mathbf{V}^T\mathbf{V}$ as:

$$\mathbf{V} = \mathbf{U}\mathbf{\Sigma}\mathbf{W}^T \tag{1}$$

Here, $\mathbf{U}$ is a matrix whose columns $\mathbf{\Psi}_i$ contain the POD spatial modes that form the orthonormal basis of $\mathbf{V}$, which are also the eigenvectors of $\mathbf{V}^T\mathbf{V}$. The diagonal matrix $\mathbf{\Sigma}$ contains the principal values σ_i of $\mathbf{V}$, which correspond to the squared eigenvalues of $\mathbf{V}^T\mathbf{V}$, thus solving the eigensystem of the time-averaged correlation matrix.

Using this formalism, numerous authors decomposed the flow field into its principal components, showing the contribution of each flow structure to the total flow field [69, 70], thus addressing many combustion issues in ICEs. For instance, Chen et al. [71] used POD to analyze misfires in spark-ignition engines, cycle-to-cycle variation was widely studied by Bizon et al. [72] and Dandby et al. [73] tracked the evolution of different species along the engine cycle. Nonetheless, it was not until Torregrosa et al. [25] when this technique was applied to the acoustic analysis of ICEs. Clear three-dimensional pressure modes were identified, reminiscent of classical open chamber acoustic modes [17] but demonstrating for the first time the additional complex interaction of the pressure waves in the different zones of the engine cylinder. Besides, they showed the energy share associated with each acoustic mode, thereby displaying a complete characterization of the acoustic distribution using POD.

3. Numerical model validation

Prior to analyzing the numerical solution, it is of utmost importance to properly validate the obtained results. For this purpose, the steady operation condition defined in Table 3 was selected.

The validity of the results was judged by the uncertainty analysis proposed in [74] and later used by Probst et al. [75] to estimate the minimum number of LES cycles that correctly captures the CCV levels in a conventional spark-ignition engine. In these works, the uncertainty due to the number of engine cycles sampled was studied in both the mean and the variation. Therefore, several consecutive engine cycles (8 in total) were calculated using both model setups. Both configurations started from the same thermodynamic conditions to allow a fair comparison of all simulated cycles whereas the first cycle was removed from the analysis to avoid inconsistencies due to possible convergence issues.

Table 3: *Details of the operating point considered in this work.*

Engine speed [rpm]	2400		
Torque [Nm]	168.3		
Number Injections [-]	3 (2 pilots + main)		
Injected mass [mg/str]	2.0	2.0	27.5
Injection timing [deg]	-36.3	-14.1	-0.1
Injection pressure [MPa]	80		
Intake pressure [MPa]	0.206		

According to Lipson [74], the true means and variations of the experiments and simulations must overlap to claim that the model is capturing the same level of CCV observed in the experiments. Full details about this statistical method are widely explained in [74]. This procedure was applied after each cycle simulation until the aforementioned statistical test was fulfilled, thereby giving the minimum number of required cycles that ensures statistically valid results.

The three parameters included in Fig. 2 were considered for the study: the peak cylinder pressure, the pressure unsteady intensity (accounting for the intensity of unsteady pressure oscillations [53]) and the noise level [76]. The latter two parameters, being exclusively used in the field of acoustics, account for the energy gathered in the high-frequency and the broadband spectra, respectively. Results included in this figure correspond to the statistics achieved after each simulated cycle (8 in total removing the first simulated cycle).

As it can be seen, experiment and simulation mean/variation overlapped after the 4th engine cycle in all considered parameters. This means, that the uncertainty of the simulations is similar to that observed in the experiments so that the solution reasonably reproduces experimental data. Therefore, results demonstrate that a statistically valid LES solution can be achieved after four realizations (cycles).

On the contrary, there are some parameters in which the means and especially the variations do not completely overlap between experiments and URANS results. For instance, the means of the peak pressure does not completely intersect, whereas the standard deviation of none of the parameters overlaps with the experimental values. These results confirm

that turbulence-driven cyclic variability cannot be modeled within the URANS context of ensemble-averaging of the fields. Nevertheless, as in the LES solution, a clear convergence is achieved after the 4th engine cycle.

In addition to the statistical analysis, the numerical solutions were directly compared against the measurements performed in the engine. All engine cycles simulated by both turbulence approaches were considered for this analysis.

In Fig. 3, the in-cylinder pressure data from a selected experimental cycle (the most representative one [77]), including the experimental standard deviation data, is plotted against the numerical solution obtained from the two simulations. In general, both models offer a good estimation of the in-cylinder pressure behavior since all simulated cycles are gathered within the experimental dispersion. Only a slight overestimation is observed in the URANS solution after top dead center when the energy release of the mixing-controlled combustion phase enhances its maximum value. Nonetheless, the gap between the experimental standard deviation and simulated cycles is small, thereby the solution can be considered sufficiently accurate. Focusing on the zoomed views, it is possible to see how the resonant oscillation is self-similar from cycle to cycle: the cyclical dispersion is limited and the same oscillation peaks can be consistently identified. Moreover, this cyclic variation is apparently reproduced only by LES.

In addition to the in-cylinder pressure comparison, the rate of heat release (HRR) is also included in Fig. 3 for deeper validation of the combustion process. Again a good match between experimental and simulated data is obtained. Although there are some differences between them, especially during the diffusion combustion phase, trends are reasonably reproduced and ignition delays are well-captured in both approaches. Moreover, the cyclic dispersion, more apparent during the main combustion where turbulence-spray interactions have a direct impact on the energy release, is again solely imitated by LES modeling.

In Fig. 4, pressure spectral density is shown, indicating the source mechanism of each part of the spectral signature, following the method presented by Strahle [78] where the mechanical compression and mean combustion pressure trace are subtracted to identify the cut-off frequency (in this case $\sim$ 4 kHz) above which the unsteady pressure oscillations are preponderant.

It can be seen in the plot that all simulated data in this last part of the spectrum is within the experimental standard deviation, suggesting that CI combustion-generated wave interaction is well captured by both turbulence approaches considered in this study. The medium frequency range, gathered by 0.4 and 4 kHz, evidences a certain degree of disagreement. However, both the main trend and the average spectral content are similar, thus validating the CFD solution.

The noise level was computed for all experimental cycles, resulting in a mean value of 89.61 dB with a standard deviation of 1.47 dB. As can be seen in Table 4, the mean values obtained from all simulated cycles (including both considered approaches) are within the aforementioned experimental deviation. For instance, URANS approach was rated at 89.01 dB of mean value, this is, a difference of only 0.6 dB against the experimental value, thus capturing the average behavior of the most relevant noise sources. In addition, the standard deviation values shown in the same table show that only LES are able to reproduce comparable values of noise intensity dispersion.

Comparing these values with those shown in Fig. 4, the combustion contribution to the CCV noise spectra is very low and not excessively relevant in the overall noise intensity. Similar trends are observed if we compare the values of unsteady intensity (resonance), showing that noise cyclic dispersion is produced fundamentally due to the alteration of the high frequency pressure field.

4. Results and discussion

4.1. Analysis of the non-reacting flow

Traditionally, the origin of the cyclic dispersion in ICE have been attributed to random fluctuations in essentially all parameters related to the reacting flow through the engine. For compression-ignition engines, global and local fluctuations of the charge mass and composition, the turbulent field inside the cylinder and the stratification (spatio-temporal distribution) of the fuel/air mixture are in particular the most relevant stochastic sources of CCV. However, contrary to earlier concepts, recent studies demonstrated that cyclic variations can follow some kind of deterministic behavior. An example of this behavior may be found in the normal engine operation when a given cycle with partial burn is followed by a cycle with higher engine output due to the residual fuel remaining in the combustion chamber after the engine scavenging [79].

Following with the example, the partial unburned fuel remaining in the cylinder after the engine scavenging should be considered as additional fuel mass to be burned in the current cycle by both LES and URANS simulations. Thus, multi-cycle URANS could take into account the deterministic behavior observed in internal combustion engines. In this sense, URANS simulations will be only considered in the analysis to verify and determine the extent to which the simulations are capable of reproducing this non-stochastic behavior. Thereby, providing a view of which physical phenomena related to noise emission are being reproduced and which not.

With the aim of further understanding the CCV sources while separating their deterministic and stochastic behaviors, the engine gas exchange process will be studied in detail. Thermodynamic properties and turbulent structures inside the cylinder are analyzed to identify their effects on combustion. The combustion process itself will be analyzed separately in order to determine the final implication of these variations on combustion and subsequently, on noise emission.

In Fig. 5 the variation of the thermodynamic conditions at IVC are shown. Here, the pressure and temperature fields were spatially-averaged for computing the presented statistics. Both parameters have a direct impact on the air mass trapped inside the combustion chamber available for fuel oxidation, thereby strongly conditioning the effective engine outputs.

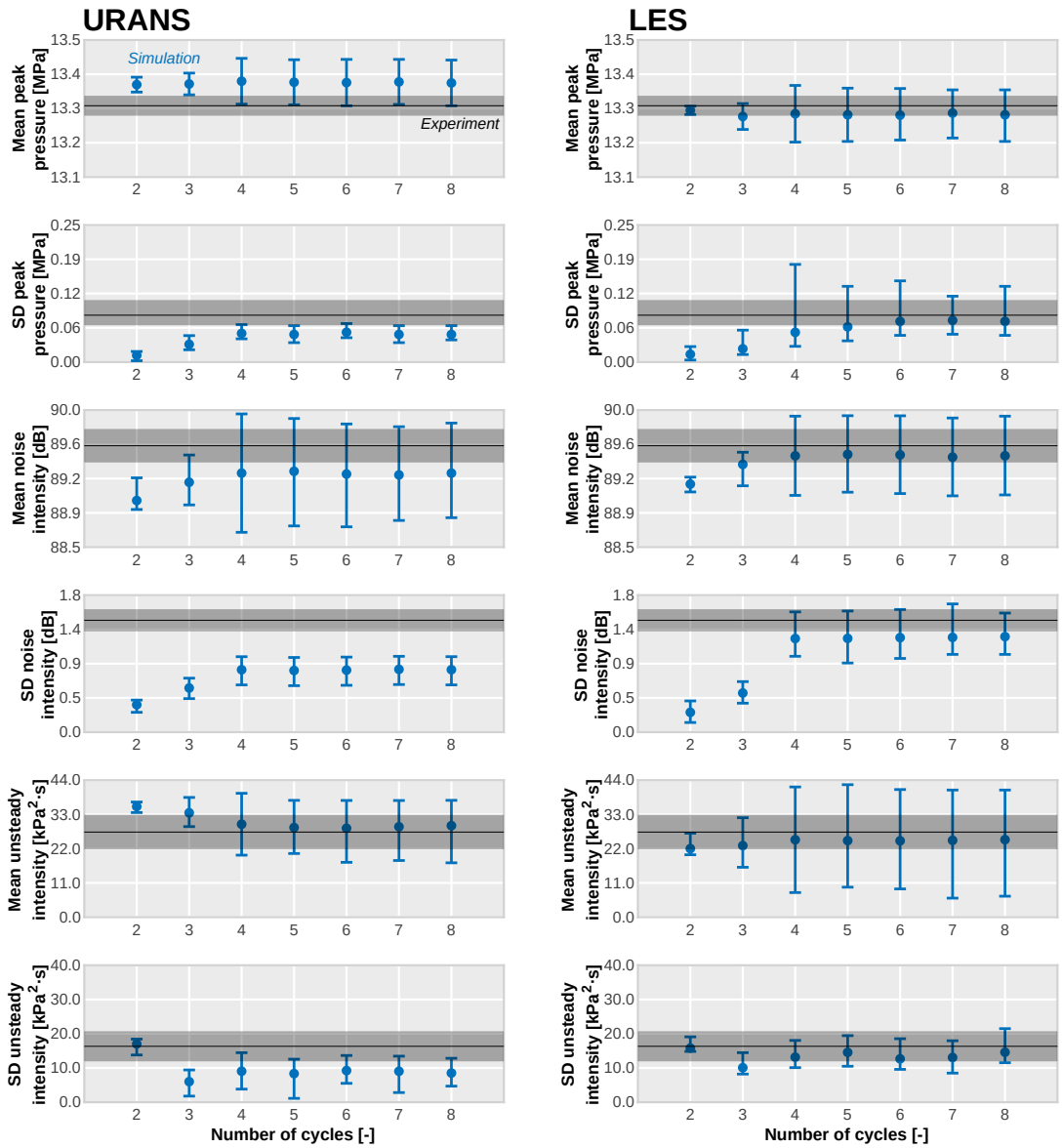

Figure 2: *Uncertainty study results. The peak cylinder pressure, the pressure unsteady intensity and the noise level were taken into account.*

In this sense, their cycle-to-cycle variability is critical for assuring stable and efficient operation. Both simulations offer similar levels of pressure variation. Moreover, these values are comparable to those obtained directly from the pressure measurements performed in the engine. However, the temperature deviation is higher for LES. As a consequence, the cycle-to-cycle variation of trapped mass is higher in LES than in URANS.

The spatial averaging can mask certain local phenomena that may be relevant in the cycle-to-cycle variability. In order to analyze the effects of local thermodynamics, the temperature fields before the start of injection are plotted for different engine cycles in Fig. 6. The selected cycles coincide with the two extreme engine cycles (with the highest and lowest cylinder pressure peak) and one intermediate (with a cylinder pressure peak similar to the cycle-averaged value). In addition to the contour slices located 1 mm away from the cylinder head, the distribution of the temperature throughout the complete combustion chamber is included by means of the probability density function (PDF).

The spatial distribution of temperature significantly changes between engine cycles when considering LES. It can be seen how the highest gradients are located at the exhaust valve side. Here, there are maximum differences of about 70K in the considered cycles. The spatial distribution also shows relevant differences between cycles. The main differences are focused on the range of 670-710K, causing a deviation of ≈4 degrees in the mean value also included as dashed lines. Contours of the URANS simulation show closer resemblance when comparing different engine cycles. There is a hot spot located at the center of the combustion chamber (slightly shifted to the exhaust valves sides) in all considered cycles. This region

Table 4: *Validation of estimated acoustic metrics.*

	Experiment		URANS		LES	
	Mean	±SD	Mean	±SD	Mean	±SD
Noise intensity [dB]	89.61	1.47	89.21	0.82	89.40	1.23
Unsteady intensity [kPa^2·s]	27.34	16.33	24.87	9.05	29.86	13.16

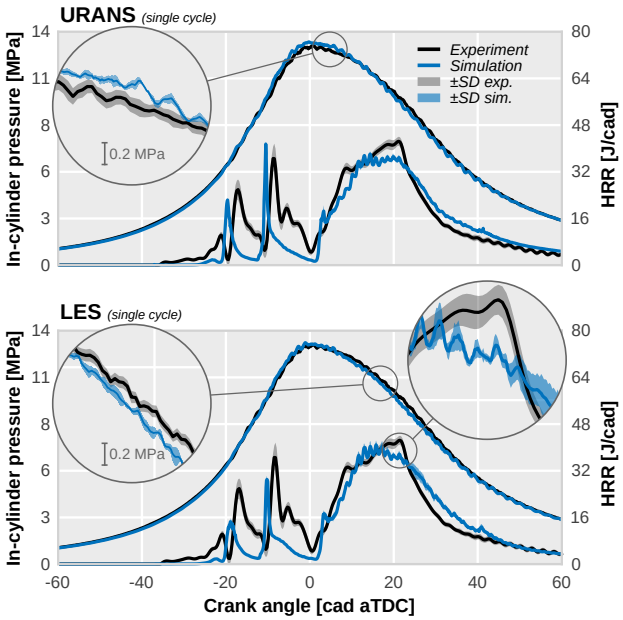

Figure 3: *Validation of the numerical models in terms of in-cylinder pressure and rate of heat release.*

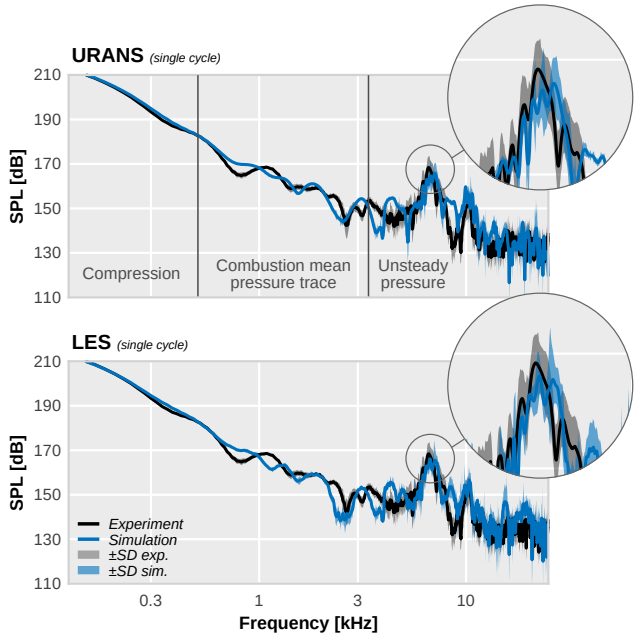

Figure 4: *Validation of the numerical models in terms of frequency content of the pressure signal.*

concentrates the highest temperature gradients, showing a maximum temperature difference of 45K. Though there are some differences in the range of 690-705K, PDFs show a high

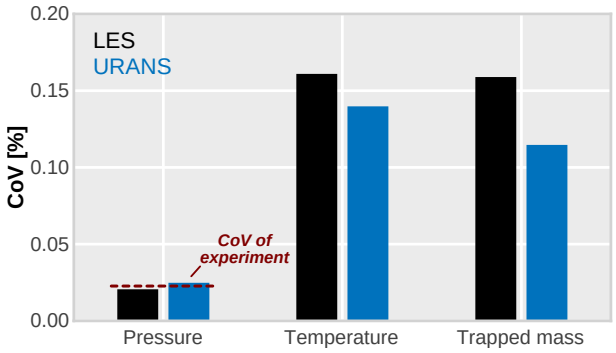

Figure 5: *Cycle-to-cycle variation of pressure, temperature and trapped mass at the intake valve closing event. The predicted levels by both simulations are compared whereas the experimental pressure variation is also included for reference.*

degree of resemblance, note that there are no dissimilarities among the mean temperatures. Comparing both simulations, the spatial distributions are also notably different. Despite that the high temperature range (> 710K) is similar between them, the distribution of lower temperatures shows a relevant disparity. LES predicts lower levels of temperature than the URANS simulation, causing a shift of 10K in the mean value.

In Fig. 7 the velocity fields of the three cycles considered so far are displayed in an attempt to identify the cycle-to-cycle differences. However, despite being extremely useful for the flow visualization, they only give a qualitative view of the flow patterns and comparing two cases directly is problematic.

A different approach has been followed to quantitatively determine the flow movement differences that conditions the combustion process. Following the example of other authors [64], the averaged swirl ratio and the distance of the vortex core to the cylinder axis were computed in order to characterize the in-cylinder air flow structures during intake and compression strokes.

The angular speed of each cell within the combustion chamber was calculated and spatially-averaged for a given crank angle to estimate the temporal evolution of SR. Results of these calculations are depicted Fig. 8 where the SR profiles for three selected cycles of both simulations are plotted. Here, the differences between LES and URANS simulations are clear. LES predicts higher levels of both SR and cycle-to-cycle dispersion during the whole engine stroke. Nevertheless, both simulations show similar profiles, showing a similar flow acceleration at the end of the compression stroke.

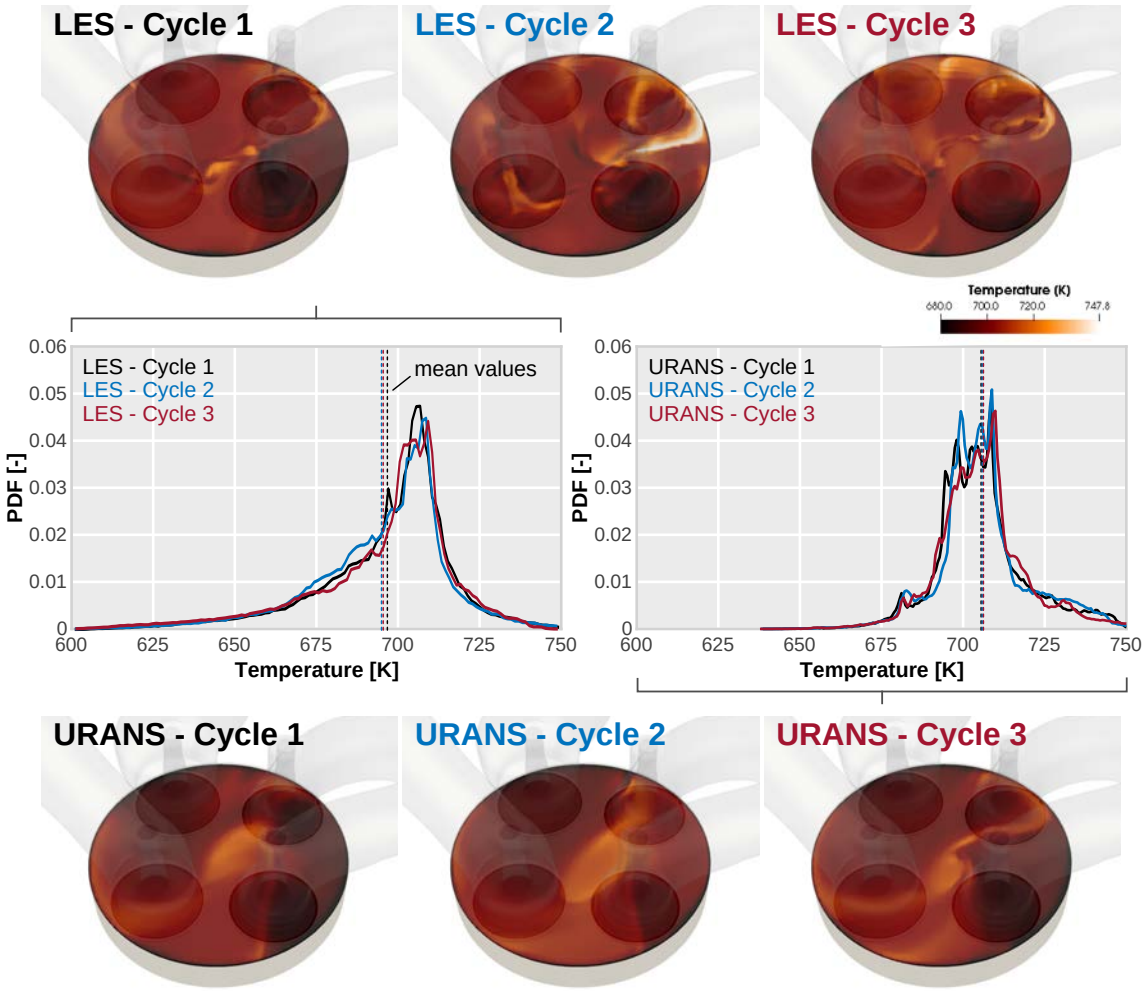

Figure 6: *Differences between LES and URANS in the temperature field prediction. Temperature contours are depicted 1 mm away from the cylinder head at the start of injection for three different cycles. The cycle with the highest cylinder pressure peak is in black, the lowest in blue and the closest to the cycle-averaged value in red. The temperature distributions within the whole combustion chamber are plotted for comparison.*

The instantaneous location of the vortex core is presented in Fig. 9. Here, computed values of the scalar function ($\Gamma(P)$) proposed by Grosjean et al. [65] are plotted in three sections of interest together with the vortex core location at a given crank angle. In addition, the velocity fields at the same regions are included to verify that the vortex core is located where this function approaches 1.

Applying this procedure at additional cross-sectional cuts it is possible to estimate the vortex core lines also included in Fig. 9. These paths give an idea about the vortex location along the cylinder axis and the variability of these among engine cycles. Therefore, following the comparison between LES and URANS results, the vortex lines were computed for

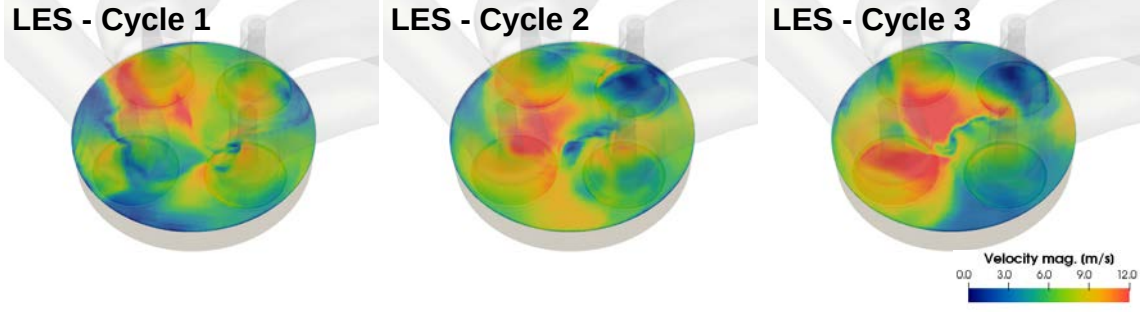

Figure 7: *Velocity fields visualization of three different engine cycles. The LES solution has been plotted in a plane perpendicular to the cylinder axis 5 mm away from the cylinder head.*

all simulated cycles. Results are summarized at the bottom plot Fig. 9, where the vortex location is given by the distance of the vortex from the cylinder center and its axial position. In this representation, solid lines are the cycle-averaged locations whereas the dashed ones represent the dispersion of this location (using the standard deviation of the radial vortex distance data). From this graph, it could be stated that there is a significant offcentering, especially when the piston is close to the Bottom Dead Center (BDC). Moreover, both modeling approaches show similar predictions in both average and variation values, only some differences are noticeable when moving towards the cylinder head. In this region, the average location diverges and both simulations predict different locations for the vortex core: LES tends predict a vortex location closer to the cylinder axis than the URANS simulation.

4.2. Analysis of combustion

Since there is still no certainty that URANS is capable of reproducing all phenomena involved in the combustion noise generation, LES is used for characterizing the combustion noise source initially. After this first characterization using LES, a comparison of the solution achieved by both approaches is done in order to establish what are the possible advantages of using URANS instead of LES modeling.

A series of snapshots were conscientiously chosen and plotted together in Fig. 10 for studying the combustion process and its effects on the internal pressure field responsible for the noise emission. They were specifically selected considering different stages of combustion to allow a better comprehension of the interaction between pressure waves and the combustion process itself.

In this figure, the pressure field (pressure oscillation) is depicted on a slice perpendicular to the cylinder axis and located 5 mm away from cylinder head. The color scale was carefully fixed for a proper visualization of pressure fluctuation. In addition, the blue edge establishes the borderline from which the pressure oscillation is bounded between 0.1 MPa and 0.15 MPa; both values were subjectively selected by taking similar values to the oscillations observed in the raw pressure trace to ensure a clear visualization of those waves

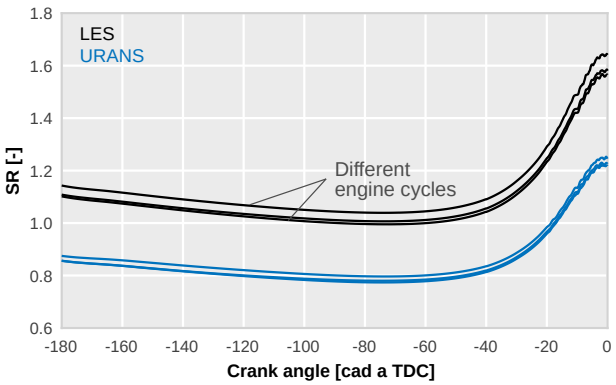

Figure 8: *Time evolution of SR of individual cycles during the compression stroke. Predictions using URANS and LES are compared for different engine cycles.*

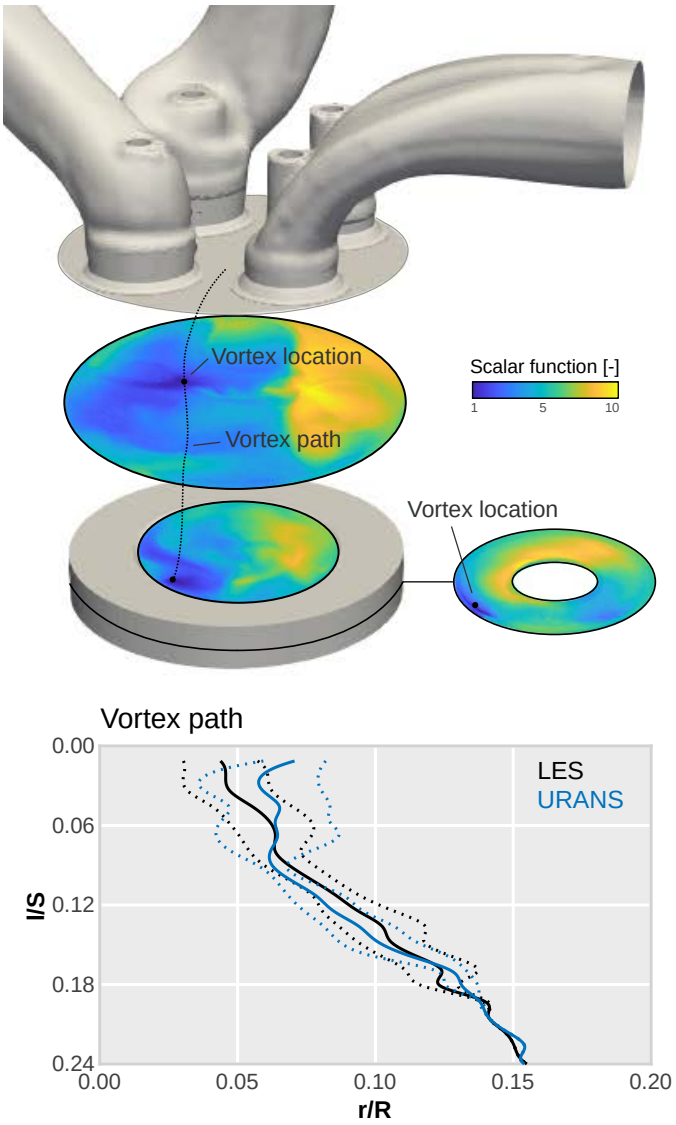

Figure 9: *Estimation of the vortex core location following the method proposed by Grosjean et al. [65].*

which become dominant. This helps to easily identify and compare the magnitude of each pressure fluctuation observed inside the chamber. The energy release profile is also included to distinguish the phase of combustion each snapshot is from. Furthermore, the Takeno flame index [80] is computed for each recorded snapshot to characterize the different combustion phases precisely. This index determines the flame regime (premixed or non-premixed) based on the spatial gradients of fuel and oxidizer concentrations. The spatially-averaged value of this index is also included for analyzing its temporal evolution.

Once fuel is injected inside the chamber, a region with high reactivity is formed at the end of the spray plume. The air-fuel mixture within this region is rapidly consumed after the spontaneous ignition, causing a sudden energy release. Then, if the fuel is still being injected, a stationary jet is established and the burning rate is now dominated by the turbulent transport.

In both combustion stages, the energy release causes an increase of temperature that subsequently contributes to rise of the mean pressure of the chamber whereas the structure of the pressure field is modified.

Snapshots displayed in the first row of Fig. 10 show the instants after the first pilot ignition, in which practically all fuel is consumed under premixed conditions (note that the Takeno flame index is above 1 during this combustion phase). It can be seen from this sequence how a pressure wave is travelling from the top-right to the bottom-left side of the chamber. As soon as this wave reaches cylinder walls it is reflected, producing a standing wave that modifies local pressure magnitudes following the already known oscillation patterns [17]. It is important to note that this resulting wave exceeds the colour scale, thus evincing that its amplitude is, at least, similar to the oscillation size observed in the transducer-registered signal.

After this first combustion phase, the second pilot burning, again mostly developing under premixed conditions, contributes to enhancement of the generated standing wave. As can be seen in snapshot 4, the narrowing of the blue borderline suggests an increase of the steepening of spatial pressure gradients related to the wave and consequently an increment of the maximum amplitude.

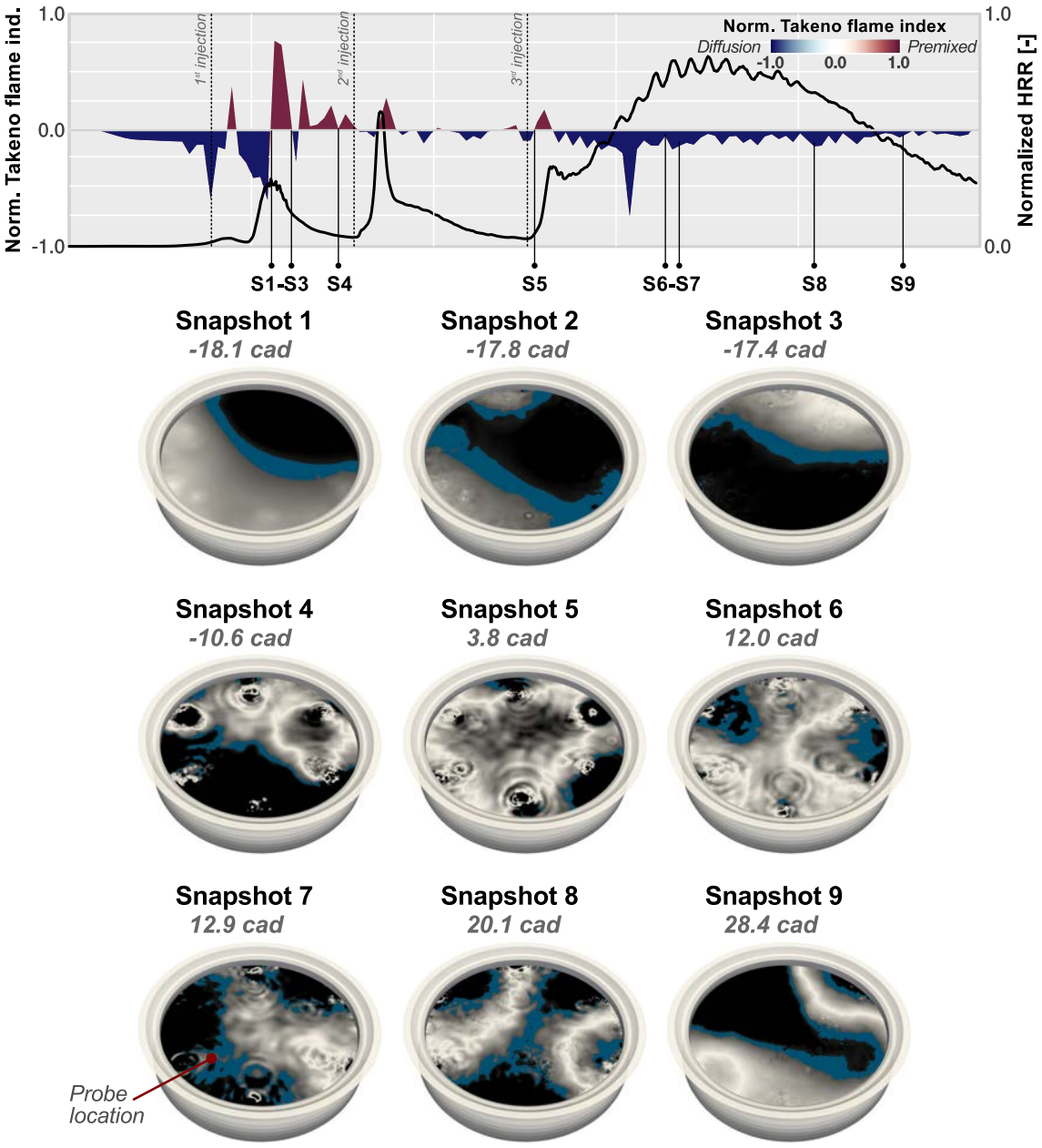

Figure 10: *Pressure field visualization during the combustion process. The spatially-averaged pressure evolution in the chamber is subtracted in order to clearly observe the unsteady pressure fluctuations.*

The following snapshot 5, which is focused on the premixed phase of the main injection burning, shows a particular and interesting phenomenon. Here, it is possible to identify the local pressure rise generated by the jets due to the premixed combustion.

Focusing on the right side of the snapshot, it can be seen how pressure waves produced at this stage practically reach the amplitude of the blue borderline. The location of the referred sprays –within the exhaust side of the chamber– suggests that there are significant differences in the spray ignition sequence. The jets positioned at the exhaust side of the chamber ignite earlier contributing not only to the unsteadiness of the in-cylinder pressure field but also to generate multiple asymmetries [52].

From here to the end of combustion (snapshots 6 to 8), the pressure field becomes slightly different and other acoustic sources appear. The turbulent interaction between the chamber atmosphere and jets acts as a supplementary source of pressure perturbations which contribute to the combustion acoustics in a similar way to what occurs in continuous flux combustors [6, 81, 82]. The heat release by the stabilized flame results in a fluctuating density that generates additional pressure waves [83]. Figure 11 shows the relative pressure evolution registered at a point located close to the quasi-steady flame (see Fig. 10). These secondary oscillations become more evident when comparing this signal during the timing of snapshot 4 (*S4*) and of snapshots 6 to 8 (*S6-S8*). The signal exhibits two fundamental oscillation frequencies, that suggest two different perturbation sources.

The standing wave generated during previous stages clearly remains as the largest pressure perturbation inside the cylinder since the maximum amplitude of the secondary oscillations are almost an order of magnitude smaller. In addition, while the standing wave persists during the whole combustion process and even when the fuel injection has finished (see snapshot 9), jet-induced oscillations are rapidly attenuated and they seldom reach to sweep the entire chamber. The contribution of these jet perturbations to the overall acoustics should be very small if it is compared not only with the uniform pressure rise but also with the resonant standing waves.

4.3. Effects of turbulence on combustion noise sources

Although it has been shown that URANS schemes offer a good estimation of in-cylinder acoustic field, including some qualitative behavior on CCV, it is still unclear if they are able to reproduce all combustion features meaningful for noise emission and captured by LES. Therefore, a comparison of both solutions is presented in this section with the target of determining the main differences between the two modeling approaches.

As in Fig. 10, the pressure gradient over a given plane is again utilized to visualize the unsteady pressure field in Fig. 12. Three snapshots were specifically chosen to compare both solutions. The first snapshot of this figure shows the spatial distribution of the pressure gradient after the first pilot burning. It can be seen how the standing wave is well-captured by both simulations, showing very similar spatial patterns.

However, the second set of snapshots which correspond to the transition from premixed to diffusion phases of the main injection burning evinces some relevant differences. As commented before for LES, the premixed combustion generates a rise of the local pressure at the end of spray plumes. Moreover, several sinks of pressure waves are located inside the jets. As the latter set of snapshots reveal, the number of these sinks increases within the spray as the diffusion flame is completely established, forming the oscillating structure already reported in several works [84, 85]. This structure is characterized by opposed amplitude regions along the spray axis as result of a helical 3D oscillation pattern [86, 87].

Focusing on the URANS solution, the equivalent instants are slightly different. While the localized pressure increment caused by the premixed burning is similar (in both pressure amplitude and location) to that observed in LES, spray pressure sinks are not clearly appreciated, at least during the transition between combustion regimes displayed in the second set of snapshots. The internal structure of sprays are however quite similar once the diffusion regime is fully stabilized. As it can be seen from the last snapshot of the URANS solution, pressure patterns are comparable between both solutions.

Although these perturbations generate a series of small pressure waves in the spray surroundings of the LES solution, they are rapidly attenuated in the URANS case, being especially difficult to visualize them if the color scale is kept among both sets of results. Since the grid resolution is similar in both setups, the main factor behind an under-estimation of gradients and the acoustic sources should be related to the underlying nature of the URANS approach that aims at predicting phase-averages, in difference to LES that relies on a spatial filtering and models only unresolved scales.

Despite this fact, the standing pressure wave developed during the first stage of combustion is still appearing in both solutions with similar magnitudes, evincing again the small relevance of these jet-induced perturbations in CI combustion acoustics.

In order to examine the differences in the combustion process itself, temperature contours at the same snapshots/planes considered in the previous figure are included in Fig. 13. Here, the number of dissimilarities is considerably higher. While the flame movement owing to larger turbulent scales are clearly visible in LES, such details are smoothed out in the URANS solution.

As a result of the interaction between the spray, in-cylinder flow and chamber walls, the flame structure is deformed in such a way that some flame sections come completely detached. As a consequence, the isolated hot spots are moved by turbulent vortexes, drawing the characteristic movement of the eddy wakes viewed in LES snapshots.

In the URANS case, these structures are not captured at the same level but they still give an idea about the temperature field change. For instance, the anti-counter-clock wise swirl movement is evident in both solutions and the flame structure is similar at the near-wall locations.

4.4. Combustion noise source characterization

According to the previous analysis, differences between URANS and LES are mainly focused on the pressure oscillations caused during the non-premixed combustion phase. Based on qualitative observations, these oscillations are small and rapidly attenuated. However, their real contribution to the internal acoustics of the combustion chamber is still unclear.

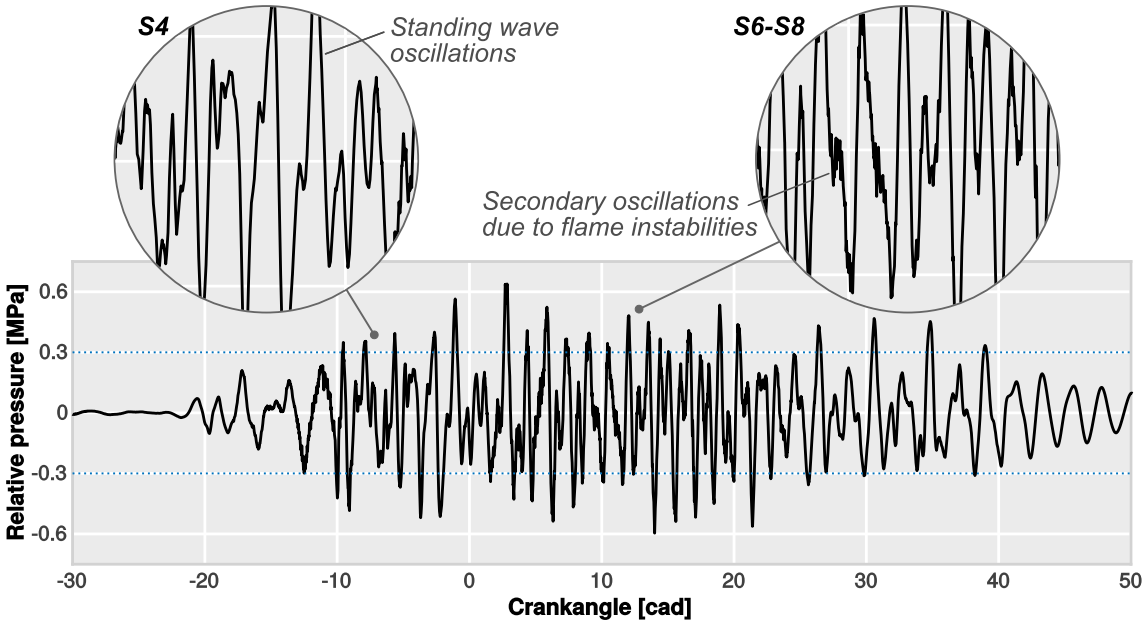

Figure 11: *The relative pressure signal resisted at a point close to the quasi-steady diffusion flame.*

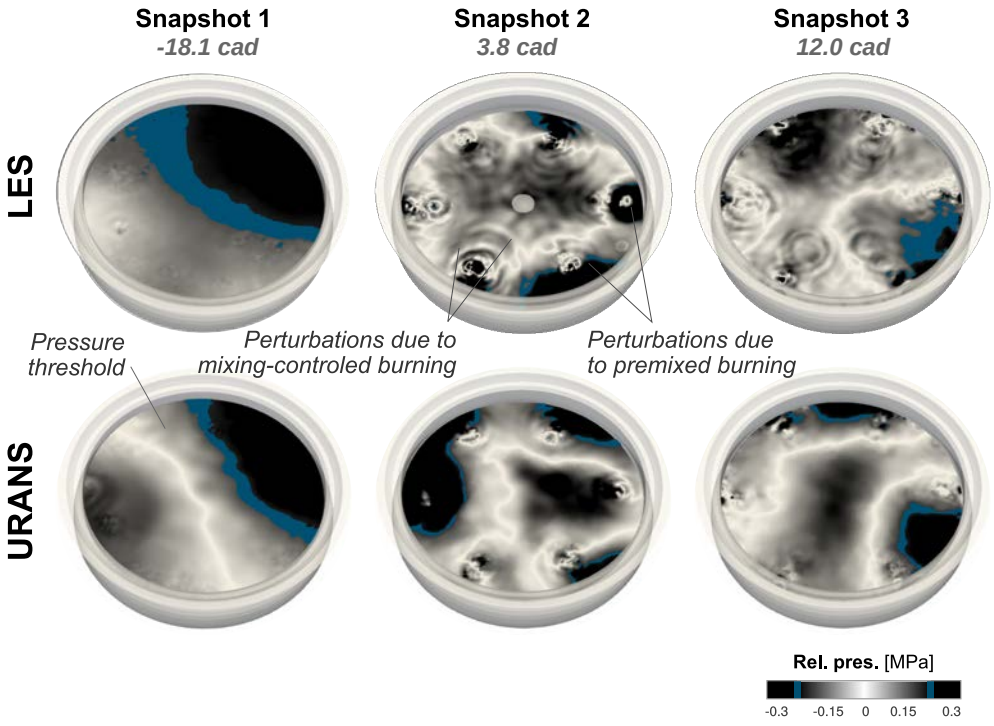

Figure 12: *Comparison of pressure field prediction using URANS and LES simulations. The spatial averaged pressure evolution in the chamber is subtracted in order to visualize unsteady pressure fluctuations.*

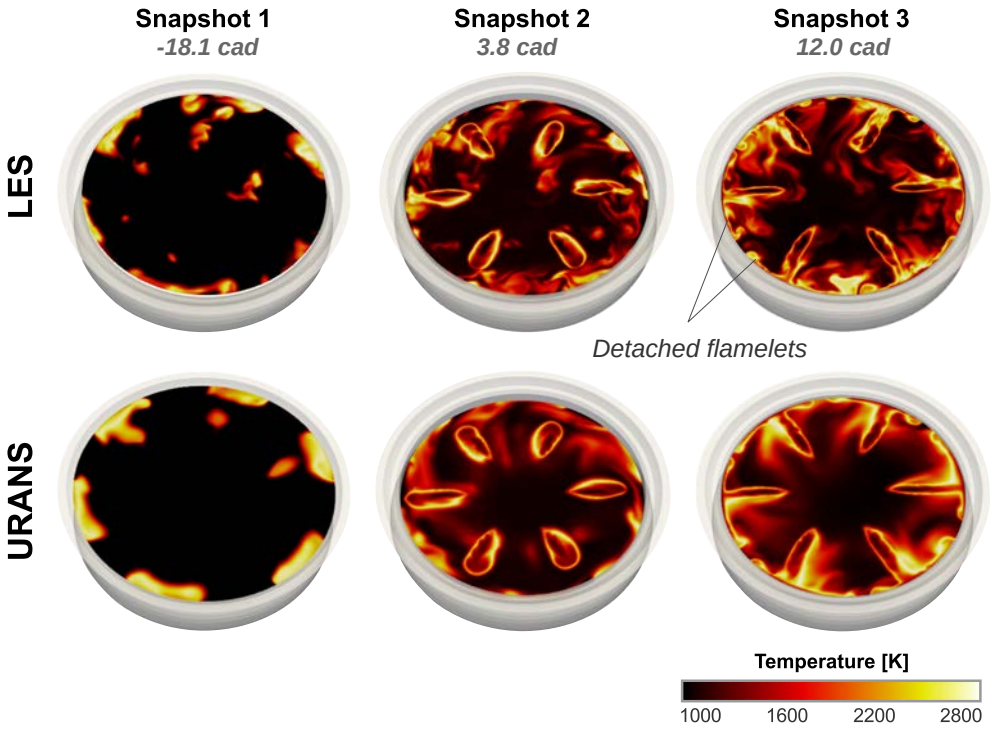

Figure 13: *Differences in local temperature field using URANS and LES approaches. Temperature contours are depicted for specific snapshots and planes.*

Proper Orthogonal Decomposition (POD) allows the identification of which spatial structures comprise the most energy of the flow field, which is understood as the superposition of all acoustic modes [88]. In order to characterize the relevance of each mode, their contributions to the total energy are computed with the help of the principal values following the methodology proposed by Torregrosa et al. [25]. Data from a given cycle was recorded at a constant time step using a frequency sampling of 48kHz for keeping all relevant acoustic information. Then, the pressure field was interpolated to a regular mesh. Therefore, the total acoustic energy within the combustion chamber is distributed as shown in the Pareto chart of Fig. 14. The accumulated energy of each simulation is normalized by the maximum total energy reached by both simulations. As LES captured higher acoustic sources, the reference value for the normalization was that obtained from the LES solution. Note that the first POD mode related to the mean homogeneous pressure (non-spatial pressure variation) is discarded to focus on the analysis of the unsteady behavior of combustion, rather than that of compression-expansion cycle. Results presented in this figure correspond to the cycle-averaged values.

Inspection of the POD mode distributions reveals that the first 8 modes gather approximately 50% of the acoustic energy. Furthermore, the level of acoustic energy accumulated by these modes is almost coincident in both simulations. Continuing with this comparison, Fig. 15 shows the spatial distribution of the four most energetic POD modes obtained from URANS and LES results. The upper and lower 10% tails (this is, the 10% and 90% percentiles) of the distribution of their real values were used to depict the characteristic set of isosurfaces of a given POD mode. It can be seen in this figure that POD modes exhibit length scales similar to both cylinder and/or bowl diameter, being similar to the structures reported by Hickling [17]. Moreover, the structures are very similar in both solutions, showing that URANS simulation is also able to reproduce the most energetic acoustic structures.

However, recalling the accumulated trends shown in the Pareto chart of Fig. 14, it can be seen how the POD energy distribution changes significantly after the POD mode 8. Both lines diverge substantially within the range gathered by POD modes Ψ_{9-27}. Here, URANS modes contain slightly higher energy than LES ones. Although not shown in this graph, these modes have large scale lengths (similar to the bowl size). From mode Ψ_{28} on, the trend is the opposite and both lines tend to converge. Here, LES modes show higher acoustic energy than URANS, compensating for the loss observed in the previous modes.

In order to identify the root cause of this difference in energy distribution, the spatial distribution of three relevant POD modes are included in Fig. 14. In this case, we used a different representation method for visualization; each mode is depicted by a contour slice of the real values of each individual mode. The most energetic POD mode Ψ_2 is characterized by a side-to-side oscillation pattern, already observed by several authors, in both simulation approaches. The mode Ψ_7 has a pattern with a higher complexity. Though they are not completely analogous, mainly caused by the visualization method,

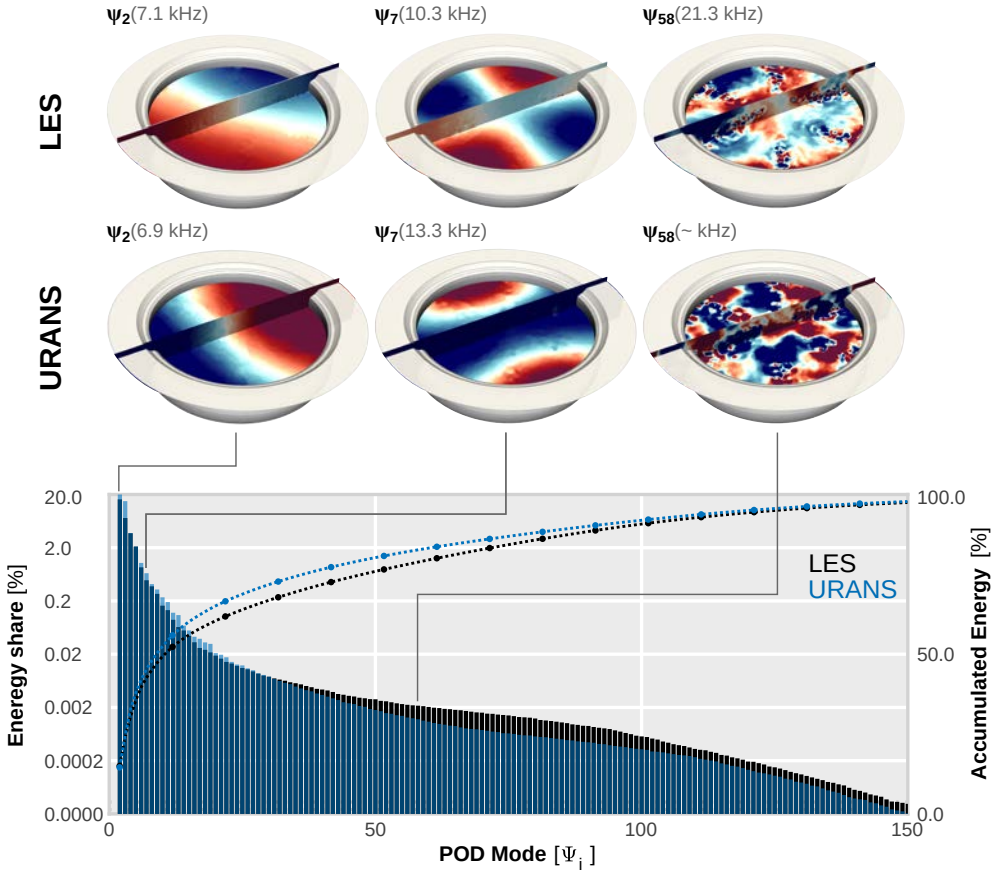

Figure 14: *Pareto chart showing the singular values associated with POD modes and the accumulated contribution to the acoustic energy.*

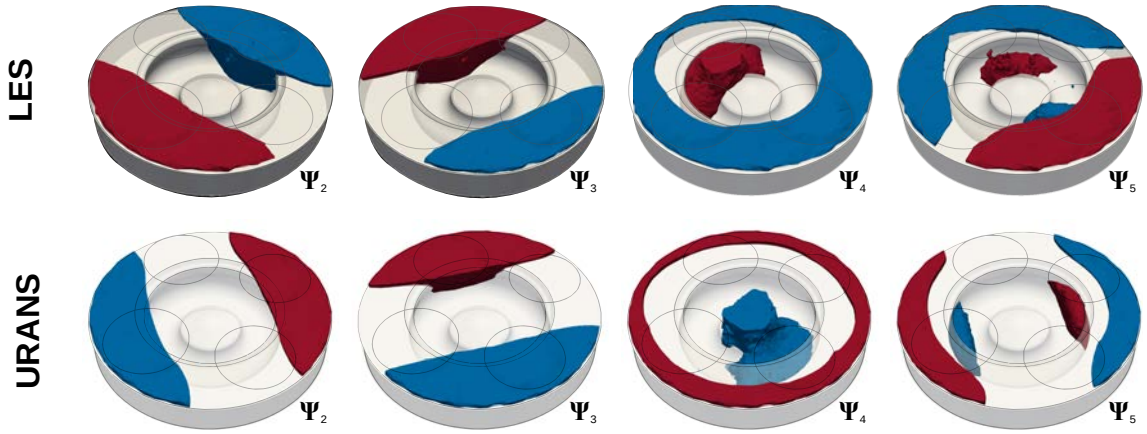

Figure 15: *Spatial distribution of the four most energetic POD modes. Each mode is represented by coloured isovolumes indicating the 10% (blue) and 90% (red) percentiles of the distribution of the real values of each individual mode. The geometry of the piston head and the position of the valves are added for reference.*

both simulations show the same transversal asymmetric mode, traditionally related to mode (m = 2, n = 0) by Hickling et al. In both cases (Ψ_2 and Ψ_7), the oscillation structures have a characteristic size comparable to the engine bore.

Differences among both simulation results arise in the POD mode Ψ_{58}. Here, LES shows a clear oscillation pattern gathered in the jet plumes. These structures have opposed amplitude regions through the jet axis as a result of the fluctuating density in the stabilized flame oscillating at a high frequency (21.3 kH). However, results from URANS simulation do not show a clear oscillation pattern focused on the reacting jets. In this case, the maximum amplitude regions do not follow a coherent structure and the characteristic frequency of this mode is not clear, being an overlap of frequencies with similar amplitudes.

In view of the results, URANS reasonably predicts up to 50% of the acoustic energy inside the combustion chamber. However, the use of LES offers higher level of accuracy since it captures additional acoustic structures throughout the whole frequency range.

5. Conclusions

In this paper, an evaluation of different modeling approaches for assessing combustion noise sources in a CI engines has been performed, with the aim of determining the impact of turbulence on the internal acoustic field recreation.

Numerical simulations have proved to be a valuable tool to extent the knowledge about all phenomena involved in the combustion noise generation, thereby overcoming experimental limitations while addressing this elusive phenomenon. The CFD solution allows a complete spatio-temporal recreation of the unsteady pressure field within the combustion chamber, which is the principal cause of the noise emission towards the cabin, but also of the spectral signature of the engine.

It has been shown how URANS simulations offer a raw estimation of in-cylinder acoustic field, resolving the pressure spectral content reasonably and predicting noise levels comparable to those emitted by the engine. On the other hand, LES have shown enhanced estimation of the cycle-to-cycle dispersion, especially when the fuel burning is dominated by the turbulent interaction within the spray, with an important counterpart in terms of computational requirements. Therefore, the use of hybrid URANS/LES approaches [89, 90] could be an interesting option to evaluate in future investigations.

Further analyses revealed that the main differences between using both modeling approaches are focused on the acoustic perturbations generated around the diffusion flame during the non-premixed combustion stage. These local density fluctuations around the diffusion flame, which spontaneously appears along the stabilized flame, are only reproduced by LES whereas URANS simulations only reproduce the sudden increase in pressure at the end of the fuel spray plumes, that generates a resonant wave inside the chamber.

Qualitative observations show that these diffusion-induced oscillations are small and rapidly attenuated, when compared to the standing wave generated due to the premixed burning. However, more in-depth analysis based on proper orthogonal decomposition methods revealed how URANS only reproduces the acoustic energy and their respective oscillation structures up to a given extent. The remaining energy is not distributed in the same way as in the LES solution, mainly due to the unpredicted jet-induced pressure oscillations.

As a consequence of this, the choice of the turbulence model is a critical aspect for noise modeling in CI engines. Despite the incapacity for reproducing those jet-induced oscillations, URANS schemes predict a raw estimation of the internal acoustic field with the added value of being computationally less expensive. Nevertheless, the use of more complex turbulence approaches (LES) offers an accurate prediction of the acoustic structures and their cyclic dispersion. In any case, both approaches contribute to the combustion noise source characterization in IC engines, helping to reduce noise levels while improving the subjective or psychoacoustic perception.

Acknowledgements

The equipment used in this work has been partially supported by FEDER project funds “Dotación de infraestructuras científico técnicas para el Centro Integral de Mejora Energética y Medioambiental de Sistemas de Transporte (CiMeT)” [grant number FEDER-ICTS-2012-06], framed in the operational program of unique scientific and technical infrastructure of the Spanish Government.

The submitted manuscript was created partly by UChicago Argonne, LLC, Operator of Argonne National Laboratory. Argonne, a U.S. Department of Energy Office of Science laboratory, is operated under Contract No. DE-AC02-06CH11357. This research was partly funded by U.S. DOE Office of Vehicle Technologies, Office of Energy Efficiency and Renewable Energy under Contract No. DE-AC02-06CH11357. The authors wish to thank Gurpreet Singh and Michael Weismiller, program managers at DOE, for their support. In addition, the authors would like to acknowledge the Laboratory Computing Resource Center (LCRC) at Argonne National Laboratory for computing time on the Bebop cluster that was used in this research.

The authors want to express their gratitude to CONVERGENT SCIENCE Inc. and Convergent Science GmbH for their kind support for the CFD calculations with the CONVERGE software.

Compliance with ethical standards

Conflict of Interest The authors declare that they have no conflict of interest

References

[1] I. Ekici, H. Bougdah, A Review of Research on Environmental Noise Barriers, Building Acoustics 10 (4) (2003) 289–323. doi:10.1260/135101003772776712.

[2] A. A. Saadu, R. O. Onyeonwu, E. O. Ayorinde, A. Ogisi, Road traffic noise survey and analysis of some major urban centers in Nigeria, Noise Control Engineering Journal 46 (1998) 146–158. doi:10.12691/wjee-1-1-2.

[3] V. R. Deulgaonkar, S. P. Kallurkar, A. G. Mattani, Review and Diagnostics of noise and vibrations in automobiles, International Journal of Modern Engineering Research 1 (2) (2011) 242–246.

[4] D. V. Matijević, V. M. Popović, Overview of modern contributions in vehicle noise and vibration refinement with special emphasis on diagnostics, FME Transactions 45 (3) (2017) 448–458.

[5] A. Schwarz, J. Janicka, Combustion Noise, Springer-Verlag, 2009. doi:10.1007/978-3-642-02038-4.

[6] F. Grimm, D. Ohno, S. Werner, M. Stöhr, R. Ewert, J. Dierke, B. Noll, M. Aigner, Direct combustion noise simulation of a lean premixed swirl flame using stochastic sound sources, 54th AIAA Aerospace Sciences Meeting, AIAA SciTech Forum (2016-1881). doi:10.2514/6.2016-1881.

[7] E. Rolland, F. De Domenico, S. Hochgreb, Direct and indirect noise generated by entropic and compositional inhomogeneities, Journal of Engineering for Gas Turbines and Powerdoi:10.1115/1.4039050.

[8] D. G. Crighton, A. P. Dowling, J. E. F. Williams, M. Heckl, F. G. Leppington, Thermoacoustic Sources and Instabilities, Springer London, London, 1992, pp. 378–405. doi:10.1007/978-1-4471-0399-8_13.

[9] A. P. Dowling, Acoustics of unstable flows, Theoretical and applied mechanics 1996 (1997) 171–186.

[10] C. L. Morfey, Amplification of aerodynamic noise by convected flow inhomogeneities, Journal of Sound and Vibration 31 (4) (1973) 391–397. doi:10.1016/S0022-460X(73)80255-X.

[11] F. E. Marble, S. M. Candel, Acoustic disturbance from gas non-uniformities convected through a nozzle, Journal of Sound and Vibration 55 (2) (1977) 225–243. doi:10.1016/0022-460X(77)90596-X.

[12] F. D. Domenico, E. O. Rolland, S. Hochgreb, Detection of direct and indirect noise generated by synthetic hot spots in a duct, Journal of Sound and Vibration 394 (2017) 220–236. doi:10.1016/j.jsv.2017.01.004.

[13] G. Persico, P. Gaetani, A. Spinelli, Assessment of synthetic entropy waves for indirect combustion noise experiments in gas turbines, Experimental Thermal and Fluid Science 88 (2017) 376–388. doi:10.1016/j.expthermflusci.2017.06.012.

[14] S. Busch, K. Zha, P. C. Miles, Investigations of closely coupled pilot and main injections as a means to reduce combustion noise in a small-bore direct injection Diesel engine, International Journal of Engine Research 16 (1) (2015) 13–22. doi:10.1177/1468087414560776.

[15] S. Busch, K. Zha, A. Warey, F. Pesce, R. Peterson, On the Reduction of Combustion Noise by a Close-Coupled Pilot Injection in a Small-Bore Direct-Injection Diesel Engine, Journal of Engineering for Gas Turbines and Power 138 (10) (2016) 102804. doi:10.1115/ICEF2015-1004.

[16] T. Fuyuto, M. Taki, Noise-canceling spike between pilot and main-pressure-rise peaks of multiple-injection diesel combustion, International Journal of Engine Research 20 (7) (2019) 788–804.

[17] R. Hickling, D. A. Feldmaier, S. H. Sung, Knock-induced cavity resonances in open chamber Diesel engines, The Journal of the Acoustical Society of America 65 (5) (1979) 1474–1479. doi:10.1121/1.382910.

[18] T. Priede, Relation between form of cylinder-pressure diagram and noise in diesel engines, Proceedings of the Institution of Mechanical Engineers: Automobile Division 14 (1) (1960) 63–97. doi:10.1243/pime_auto_1960_000_012_02.

[19] A. J. Torregrosa, A. Broatch, X. Margot, V. Marant, Combustion chamber resonances in direct injection automotive Diesel engines: a numerical approach, International Journal of Engine Research 5 (1) (2003) 83–91. doi:10.1243/146808704772914264.

[20] L. J. Eriksson, Higher order mode effects in circular ducts and expansion chambers, Journal of the Acoustical Society of America 68 (1980) 545. doi:10.1121/1.384768.

[21] A. Broatch, X. Margot, A. Gil, C. Donayre, Computational study of the sensitivity to ignition characteristics of the resonance in DI diesel engine combustion chambers, Engineering Computations 24 (1) (2007) 77–96. doi:10.1108/02644400710718583.

[22] A. Broatch, X. Margot, A. Gil, J. C. Donayre, A CFD approach to diesel engine combustion chamber resonance, SAE Technical Paper 2007-24-0043. doi:10.4271/2007-24-0043.

[23] P. Olmeda, J. Martín, R. Novella, D. Blanco-Cavero, Assessing the optimum combustion under constrained conditions, International Journal of Engine Research 21 (5) (2020) 811–823.

[24] A. J. Torregrosa, A. Broatch, X. Margot, J. Gomez-Soriano, Understanding the unsteady pressure field inside combustion chambers of compression ignition engines using a CFD approach, International Journal of Engine Research 21 (8) (2020) 1273–1285. doi:10.1177/1468087418803030.

[25] A. J. Torregrosa, A. Broatch, J. García-Tíscar, J. Gomez-Soriano, Modal decomposition of the unsteady flow field in compression-ignited combustion chambers, Combustion and Flame 188 (2018) 469–482. doi:10.1016/j.combustflame.2017.10.007.

[26] T. Schuller, O. Sauvage, Z. Dimitrijevic, G. Rymer, Acoustic Analysis of Unsteady Diesel Engine Combustion Chamber Pressure Evolution, 11th AIAA/CEAS Aeroacoustics Conference (2005) 2910doi:10.2514/6.2005-2910.

[27] A. Robert, K. Truffin, N. Iafrate, S. Jay, O. Colin, C. Angelberger, Large-eddy simulation analysis of knock in a direct injection spark ignition engine, International Journal of Engine Research 20 (7) (2019) 765–776.

[28] CONVERGENT SCIENCE Inc., CONVERGE 2.2 Theory Manual (2015).

[29] O. Redlich, J. N. S. Kwong, On the Thermodynamics of Solutions. V. An Equation of State. Fugacities of Gaseous Solutions, Chemical Reviews 44 (1) (1949) 233–244. doi:10.1021/cr60137a013.

[30] R. I. Issa, Solution of the implicitly discretised fluid flow equations by operator-splitting, Journal of Computational physics 62 (1) (1986) 40–65.

[31] S. B. Pope, Ten questions concerning the large-eddy simulation of turbulent flows, New Journal of Physics 6 (1) (2004) 35. doi:10.1088/1367-2630/6/1/035.

[32] E. Pomraning, C. J. Rutland, Dynamic one-equation nonviscosity large-eddy simulation model, AIAA journal 40 (4) (2002) 689–701. doi:10.2514/2.1701.

[33] P. K. Senecal, E. Pomraning, K. J. Richards, S. Som, An Investigation of Grid Convergence for Spray Simulations using an LES Turbulence Model, SAE 2013 World Congress & Exhibitiondoi:10.4271/2013-01-1083.

[34] V. Yakhot, S. Orszag, Renormalization group analysis of turbulence., Journal of Scientific Computing 1 (1) (1986) 3–51. doi:doi:10.1007/BF01061452.

[35] L. Pickett, G. Bruneaux, R. Payri, Engine combustion network, Sandia National Laboratories, Livermore, CA, http://www. ca. sandia. gov/ecn.

[36] P. Pal, D. Probst, Y. Pei, Y. Zhang, M. Traver, D. Cleary, S. Som, Numerical Investigation of a Gasoline-Like Fuel in a Heavy-Duty Compression Ignition Engine Using Global Sensitivity Analysis, SAE International Journal of Fuels and Lubricants 10 (1) (2017) 56–68. doi:10.4271/2017-01-0578.

[37] C. Angelberger, T. Poinsot, B. Delhay, Improving near-wall combustion and wall heat transfer modeling in SI engine computations, SAE Technical Paper 2003-01-0542. doi:10.4271/972881.

[38] P. K. Senecal, E. Pomraning, K. J. Richards, T. E. Briggs, C. Y. Choi, R. M. McDavid, M. A. Patterson, Multi-Dimensional Modeling of Direct-Injection Diesel Spray Liquid Length and Flame Lift-off Length using CFD and Parallel Detailed Chemistry, SAE Technical Paper 2003-01-1043. doi:10.4271/2003-01-1043.

[39] A. Babajimopoulos, D. N. Assanis, D. L. Flowers, S. M. Aceves, R. P. Hessel, A fully coupled computational fluid dynamics and multi-zone model with detailed chemical kinetics for the simulation of premixed charge compression ignition engines, International Journal of Engine Research 6 (5) (2005) 497–512. doi:10.1243/146808705X30503.

[40] P. Pal, S. Keum, H. G. Im., Assessment of flamelet versus multi-zone combustion modeling approaches for stratified-charge compression ignition engines, International Journal of Engine Research 17 (3) (2016) 280–290. doi:10.1177/1468087415571006.

[41] P. Pal, Computational Modeling and Analysis of Low Temperature Combustion Regimes for Advanced Engine Applications, Ph.D. thesis, University of Michigan-Ann Arbor (2016).
URL http://hdl.handle.net/2027.42/120735

[42] Y. Pei, S. Som, E. Pomraning, P. K. Senecal, S. A. Skeen, J. Manin, L. M. Pickett, Large eddy simulation of a reacting spray flame with multiple realizations under compression ignition engine conditions, Combustion and Flame 162 (12) (2015) 4442–4455. doi:10.1016/j.combustflame.2015.08.010.

[43] J. Brakora, R. D. Reitz, A Comprehensive Combustion Model for Biodiesel-Fueled Engine Simulations, SAE Technical Paper 2013-01-1099. doi:10.4271/2013-01-1099.

[44] J. K. Dukowicz, A particle-fluid numerical model for liquid sprays, Journal of Computational Physics 35 (2) (1980) 229–253. doi:10.1016/0021-9991(80)90087-X.

[45] R. D. Reitz, J. C. Beale, Modeling spray atomization with the Kelvin-Helmholtz/Rayleigh-Taylor hybrid model, Atomization and Sprays 9 (6) (1999) 623–650. doi:10.1615/AtomizSpr.v9.i6.40.

[46] P. J. O'Rourke, Collective drop effects on vaporizing liquid sprays, Ph.D. thesis (1981).

[47] A. A. Amsden, P. J. O'rourke, T. D. Butler, KIVA-II: A computer program for chemically reactive flows with sprays, Tech. rep., Los Alamos National Laboratory, NM (USA) (1989).

[48] A. B. Liu, D. Mather, R. D. Reitz, Modeling the Effects of Drop Drag and Breakup on Fuel Sprays, International Congress & Expositiondoi:10.4271/930072.

[49] S. Molina, A. García, J. M. Pastor, E. Belarte, I. Balloul, Operating range extension of RCCI combustion concept from low to full load in a heavy-duty engine, Applied Energy 143 (2015) 211–227. doi:10.1016/j.apenergy.2015.01.035.

[50] C. Habchi, F. A. Lafossas, P. Béard, D. Broseta, Formulation of a one-component fuel lumping model to assess the effects of fuel thermodynamic properties on internal combustion engine mixture preparation and combustion, 2004 SAE Fuels & Lubricants Meeting & Exhibitiondoi:10.4271/2004-01-1996.

[51] A. J. Torregrosa, P. Olmeda, B. Degraeuwe, M. Reyes, A concise wall temperature model for DI Diesel engines, Applied Thermal Engineering 26 (11-12). doi:10.1016/j.applthermaleng.2005.10.021.

[52] A. J. Torregrosa, A. Broatch, A. Gil, J. Gomez-Soriano, Numerical approach for assessing combustion noise in compression-ignitied Diesel engines, Applied Acoustics 135 (2018) 91–100. doi:10.1016/j.apacoust.2018.02.006.

[53] A. Broatch, R. Novella, J. Gomez-Soriano, P. Pal, S. Som, Numerical Methodology for Optimization of Compression-Ignited Engines Considering Combustion Noise Control, SAE International Journal of Engines 2018-01-0193. doi:10.1016/2018-01-0193.

[54] S. Som, Development and validation of spray models for investigating diesel engine combustion and emissions, Ph.D. thesis, University of Illinois at Chicago (2009).

[55] S. Som, S. K. Aggarwal, Effects of primary breakup modeling on spray and combustion characteristics of compression ignition engines, Combustion and Flame 157 (6) (2010) 1179–1193. doi:10.1016/j.combustflame.2010.02.018.

[56] P. K. Senecal, E. Pomraning, K. J. Richards, S. Som, Grid-convergent spray models for internal combustion engine computational fluid dynamics simulations, Journal of Energy Resources Technology 136 (1) (2014) 012204. doi:10.1115/1.4024861.

[57] P. K. Senecal, E. Pomraning, Q. Xue, S. Som, S. Banerjee, B. Hu, K. Liu, J. M. Deur, Large Eddy simulation of vaporizing sprays considering multi-injection averaging and grid-convergent mesh resolution, Journal of Engineering for Gas Turbines and Power 136 (11) (2014) 111504. doi:10.1115/1.4027449.

[58] J. Kodavasal, C. P. Kolodziej, S. A. Ciatti, S. Som, Computational fluid dynamics simulation of gasoline compression ignition, Journal of Energy Resources Technology 137 (3) (2015) 032212. doi:10.1115/1.4029963.

[59] H. Wang, R. D. Reitz, M. Yao, Comparison of Diesel Combustion CFD Models and Evaluation of the Effects of Model Constants, SAE 2012 World Congress & Exhibitiondoi:10.4271/2012-01-0134.

[60] J. Taglialegami, G. Bogin, E. Osecky, A. M. Dean, Simulation of n-Heptane and Surrogate Fuels for Advanced Combustion Engines (FACE) in a Single-Cylinder Compression Ignition Engine, ASME 2013 Internal Combustion Engine Division Fall Technical Conferencedoi:10.1115/ICEF2013-19257.

[61] A. Oyediran, D. Darling, K. Radhakrishnan, Review of combustion-acoustic instabilities, American Institute of Aeronautics and Astronauticsdoi:10.2514/6.1995-2469.

[62] P. Pal, Y. Wu, T. Lu, S. Som, Y. C. See, A. Le Moine, Multidimensional numerical simulations of knocking combustion in a cooperative fuel research engine, Journal of Energy Resources Technology 140 (10).

[63] F. Ihlenburg, The Medium-Frequency Range in Computational Acoustics: Practical and Numerical Aspects, Journal of Computational Acoustics 11 (02) (2003) 175–193. doi:10.1142/S0218396X03001900.

[64] A. Gil, J. V. Pastor, A. Garcia, L. Pachano, Combined cfd-piv methodology for the characterization of air flow in a diesel engine, SAE Technical Paper.

[65] N. Grosjean, L. Graftieaux, M. Michard, W. Hübner, C. Tropea, J. Volkert, Combining lda and piv for turbulence measurements in unsteady swirling flows, Measurement Science and Technology 8 (12) (1997) 1523.

[66] Y. Liang, H. Lee, S. Lim, W. Lin, K. Lee, C. Wu, Proper orthogonal decomposition and its applications-part i: Theory, Journal of Sound and vibration 252 (3) (2002) 527–544. doi:10.1006/jsvi.2001.4041.

[67] J. L. Lumley, The structure of inhomogeneous turbulent flows, in: Atmospheric Turbulence and Radio Wave Propagation – Proceedings of the International Colloquium, Nauka, Moscow, 1967, pp. 166–178.

[68] S. Bagheri, Koopman-mode decomposition of the cylinder wake, Journal of Fluid Mechanics 726 (2013) 596–623. doi:10.1017/jfm.2013.249.

[69] Y. Huang, V. Yang, Dynamics and stability of lean-premixed swirl-stabilized combustion, Progress in energy and combustion science 35 (4) (2009) 293–364. doi:10.1016/j.pecs.2009.01.002.

[70] V. Caux-Brisebois, A. M. Steinberg, C. M. Arndt, W. Meier, Thermo-acoustic velocity coupling in a swirl stabilized gas turbine model combustor, Combustion and Flame 161 (12) (2014) 3166–3180. doi:10.1016/j.combustflame.2014.05.020.

[71] H. Chen, D. L. S. Hung, M. Xu, H. Zhuang, J. Yang, Proper orthogonal decomposition analysis of fuel spray structure variation in a spark-ignition direct-injection optical engine, Experiments in fluids 55 (4) (2014) 1703. doi:10.1007/s00348-014-1703-y.

[72] K. Bizon, G. Continillo, S. Lombardi, P. Sementa, B. M. Vaglieco, Independent component analysis of cycle resolved combustion images from a spark ignition optical engine, Combustion and Flame 163 (2016) 258–269. doi:10.1016/j.combustflame.2015.10.002.

[73] S. J. Danby, T. Echekki, Proper orthogonal decomposition analysis of autoignition simulation data of nonhomogeneous hydrogen–air mixtures, Combustion and flame 144 (1) (2006) 126–138. doi:10.1016/j.combustflame.2005.06.014.

[74] C. Lipson, Statistical design and analysis of engineering experiments, Tech. rep. (1973).

[75] D. Probst, S. Wijeyakulasuriya, E. Pomraning, J. Kodavasal, R. Scarcelli, S. Som, Predicting cycle-to-cycle variation with concurrent cycles in a gasoline direct injected engine with large eddy simulations, ASME 2018 Internal Combustion Engine Division Fall Technical Conference (2018) V002T06A022–V002T06A022.

[76] A. J. Torregrosa, A. Broatch, J. Martín, L. Monelletta, Combustion noise level assessment in direct injection Diesel engines by means of in-cylinder pressure components, Measurement Science and Technology 18 (7) (2007) 2131–2142. doi:10.1088/0957-0233/18/7/045.

[77] P. Pal, C. P. Kolodziej, S. Choi, S. Som, A. Broatch, J. Gomez-Soriano, Y. Wu, T. Lu, Y. C. See, Development of a virtual cfr engine model for knocking combustion analysis, SAE Int. J. Enginesdoi:10.4271/2018-01-0187.

[78] W. C. Strahle, Combustion randomness and diesel engine noise: theory and initial experiments, Combustion and Flame 28 (1977) 279–290. doi:10.1016/0010-2180(77)90033-5.

[79] T. D. Fansler, R. M. Wagner, Cyclic dispersion in engine combustion-Introduction by the special issue editors, International Journal of Engine Research 16 (3) (2015) 255–259. doi:10.1177/1468087415572740.

[80] H. Yamashita, M. Shimada, T. Takeno, A numerical study on flame stability at the transition point of jet diffusion flames, in: Symposium (International) on Combustion, Vol. 26, Elsevier, 1996, pp. 27–34. doi:10.1016/S0082-0784(96)80196-2.

[81] F. Flemming, A. Sadiki, J. Janicka, Investigation of combustion noise using a LES/CAA hybrid approach, Proceedings of the Combustion Institute 31 (2) (2007) 3189–3196. doi:10.1016/j.proci.2006.07.060.

[82] C. F. Silva, M. Leyko, F. Nicoud, S. Moreau, Assessment of combustion noise in a premixed swirled combustor via Large-Eddy Simulation, Computers & Fluids 78 (2013) 1–9. doi:10.1016/j.compfluid.2010.09.034.

[83] A. Broatch, R. Novella, J. García-Tíscar, J. Gomez-Soriano, P. Pal, Analysis of combustion acoustic phenomena in compression–ignition engines using large eddy simulation, Physics of Fluids 32 (8) (2020) 085101. doi:10.1063/5.0011929.

[84] H. Chen, M. Xu, D. L. S. Hung, J. Yang, H. Zhuang, Development of a POD-Based Analysis Approach for Quantitative Comparison of Spray Structure Variations in a Spark-Ignition Direct-Injection Engine, SAE/KSAE 2013 International Powertrains, Fuels & Lubricants Meetingdoi:10.4271/2013-01-2545.

[85] G. Tissot, L. Cordier, N. Benard, B. R. Noack, Model reduction using Dynamic Mode Decomposition, Comptes Rendus Mécanique 342 (6) (2014) 410–416, flow separation control. doi:10.1016/j.crme.2013.12.011.

[86] T. Colonius, J. Freund, POD analysis of sound generation by a turbulent jet, 40th AIAA Aerospace Sciences Meeting & Exhibit (2002) 72doi:10.2514/6.2002-72.

[87] D. M. Markovich, S. S. Abdurakipov, L. M. Chikishev, V. M. Dulin, K. Hanjalić, Comparative analysis of low- and high-swirl confined flames and jets by proper orthogonal and dynamic mode decompositions, Physics of Fluids 26 (6) (2014) 065109. doi:10.1063/1.4884915.

[88] N. Aubry, On the hidden beauty of the proper orthogonal decomposition, Theoretical and Computational Fluid Dynamics 2 (5-6) (1991) 339–352. doi:10.1007/BF00271473.

[89] C. Iacovano, A. d'Adamo, S. Fontanesi, G. Di Ilio, V. K. Krastev, Application of a zonal hybrid urans/les turbulence model to high and low-resolution grids for engine simulation, International Journal of Engine Research (2020) 1468087420931712.

[90] V. K. Krastev, A. d'Adamo, F. Berni, S. Fontanesi, Validation of a zonal hybrid urans/les turbulence modeling method for multi-cycle engine flow simulation, International Journal of Engine Research 21 (4) (2020) 632–648.